

Giant spatial anisotropy of magnon lifetime in altermagnets

António T. Costa^{1,2*}, João C. G. Henriques^{1,3} and Joaquín Fernández-Rossier^{1,4}

1 International Iberian Nanotechnology Laboratory (INL), Av. Mestre José Veiga, 4715-330 Braga, Portugal

2 Physics Center of Minho and Porto Universities (CF-UM-UP), Universidade do Minho, Campus de Gualtar, 4710-057 Braga, Portugal

3 Universidade de Santiago de Compostela, 15782 Santiago de Compostela, Spain

4 On permanent leave from Departamento de Física Aplicada, Universidad de Alicante, 03690 San Vicente del Raspeig, Spain

★ antonio.costa@inl.int,

Abstract

Altermagnets are a new class of magnetic materials with zero net magnetization (like antiferromagnets) but spin-split electronic bands (like ferromagnets) over a fraction of reciprocal space. As in antiferromagnets, magnons in altermagnets come in two flavours, that either add one or remove one unit of spin to the $S = 0$ ground state. However, in altermagnets these two magnon modes are non-degenerate along some directions in reciprocal space. Here we show that the lifetime of altermagnetic magnons has a very strong dependence on both flavour and direction. Strikingly, coupling to Stoner modes leads to a complete suppression of magnon propagation along selected spatial directions. This giant anisotropy will impact electronic, spin, and energy transport properties and may be exploited in spintronic applications.

Copyright attribution to authors.

This work is a submission to SciPost Physics.

License information to appear upon publication.

Publication information to appear upon publication.

Received Date

Accepted Date

Published Date

1

2 Contents

3	1 Introduction	2
4	2 Model and mean-field ground state	3
5	2.1 Mean-field results	5
6	3 Magnons	5
7	3.1 Itinerant altermagnet	6
8	4 Conclusion	10
9	A Mean-field electronic structure	10
10	B Relationship between the density of Stoner modes and the magnon lifetime	12
11	C Origin of the anisotropic magnon lifetime	12

12	D Insulating altermagnet in the intermediate coupling regime ($U = 3.5\tau$).	13
13	E Directionality of the magnon spectrum in the insulating regime (intermediate	
14	coupling).	14
15	References	16
16	<hr/>	
17		

18 1 Introduction

19 The recent recognition of altermagnets as a new class of magnetic materials [1–3], originally
 20 predicted by Pekar and Rashba in 1964 [4], has been a very exciting development for both
 21 condensed matter and materials physics. In a static configuration, altermagnets camouflage
 22 very well as antiferromagnets; however, when you look under the hood the disguise is given
 23 away by the spin-polarized electronic bands. It is their dynamics, however, that reveal their
 24 true colors [5, 6]. To understand the dynamical properties of a magnetic system it is essential
 25 to look at its elementary spin excitations, or magnons [7].

26 A magnon in a ferromagnetic solid is usually associated to processes by which the total mag-
 27 netization of the sample is lowered by the equivalent of a quantum of angular momentum, \hbar ,
 28 and associated with the spin-lowering operator S^- . We thus say that a ferromagnetic magnon
 29 carries spin $S^z = -1$. In terms of elementary electronic processes, generating a magnon con-
 30 sists in promoting an electron from the majority spin band (\uparrow) to the minority spin band (\downarrow),
 31 and is associated with the operator $a_{\downarrow}^{\dagger}a_{\uparrow}$. By virtue of electron-electron interactions, the elec-
 32 tron and the hole involved in this process form a bound state, whose energy depends on the
 33 net crystal momentum of the pair.

34 In antiferromagnets, magnons can have either $S^z = -1$ or $S^z = 1$, associated with lowering
 35 the spin of the \uparrow sublattice or raising the spin of the \downarrow sublattice. Due to the complete equiva-
 36 lence between the two spin directions, the two kinds of antiferromagnetic magnons ($S^z = \pm 1$)
 37 have identical energies [8]. On the other hand, it has been noted [2, 9] that magnons in alter-
 38 magnets have unique features when compared to their antiferromagnetic counterparts. The
 39 most noticeable difference is that $S^z = -1$ and $S^z = 1$ magnons have distinct energies along
 40 certain directions in the reciprocal space, the same direction associated with the spin-split
 41 electronic bands.

42 In metallic magnets, magnons have finite lifetimes, due to the fact that they can decay
 43 into uncorrelated electron-hole pairs, also known as a Stoner excitations [10, 11]. The decay
 44 probability (hence the inverse of the magnon lifetime) is proportional to the spectral density
 45 associated with the Stoner excitations, which usually increases monotonically with energy for
 46 a fixed wavevector. Thus, magnon lifetimes typically decrease monotonically as the magnon
 47 energy increases [12].

48 It has been assumed hitherto [9] that, due to the distinct energies of $S^z = \pm 1$ magnons
 49 in altermagnets, their lifetimes would also be different, in an almost trivial manner. Other
 50 works have looked into the effects of magnon-magnon interactions on magnon lifetimes, a
 51 mechanism that is supposed to be relevant for insulating magnets. [13] Apart from that, very
 52 little attention has been paid to the lifetime of magnons in altermagnets, and most theoretical
 53 approaches employ spin-only models in their description [9, 14–16].

54 Here we show that Stoner damping in metallic and slightly doped altermagnets has highly
 55 non-trivial consequences. Specifically, the combination between the peculiar symmetry of the
 56 altermagnet and the damping by Stoner excitations makes magnons in itinerant altermagnets

57 completely distinct from their antiferro- and ferromagnetic counterparts. The magnons acquire
 58 a strong frequency- and spin-dependent directionality, which can potentially be exploited as a
 59 resource in spintronics devices [17].

60 2 Model and mean-field ground state

61 We model the electronic structure of altermagnets using a Hamiltonian proposed in ref. [18],
 62 which is essentially a Hubbard model with an especially chosen hopping structure that realises
 63 an altermagnetic symmetry,

$$H = \sum_{l'l'} \sum_{\mu\mu'} \sum_{\sigma} \tau_{ll'}^{\mu\mu'} c_{l\mu\sigma}^{\dagger} c_{l'\mu'\sigma} + U \sum_{l,\mu} n_{l\mu\uparrow} n_{l\mu\downarrow}, \quad (1)$$

64 where $n_{l\mu\sigma} \equiv c_{l\mu\sigma}^{\dagger} c_{l\mu\sigma}$, l and l' label unit cells, μ and μ' label sublattices (A or B) and σ labels
 65 the spin projection along the z axis. The hopping matrix $\tau_{ll'}^{\mu\mu'}$ is described in the caption of
 66 Fig. 1. The intra-atomic interaction parameter U can be chosen to place the system in either
 67 the metallic or insulating altermagnetic phase; for the value of diagonal hopping we adopted
 68 in this work, $2\tau \lesssim U \lesssim 3\tau$ yields a metallic altermagnetic phase, whereas $U \gtrsim 3\tau$ produces
 69 the insulating altermagnetic phase. The complete mean-field phase diagram of this model
 70 has been explored in Ref. [18]. Here we will choose two representative points, one in the
 71 insulating and one in the metallic region, and study the elementary spin excitations above
 72 their respective mean-field ground states. The mean-field approximation we employ amounts
 73 to the following replacement,

$$U \sum_{l,\mu} n_{l\mu\uparrow} n_{l\mu\downarrow} \longrightarrow \frac{U}{2} \sum_{l,\mu} [(\bar{n}_{\mu l} + \bar{m}_{\mu l}) n_{l\mu\downarrow} + (\bar{n}_{\mu l} - \bar{m}_{\mu l}) n_{l\mu\uparrow}], \quad (2)$$

74 with $\bar{n}_{\mu l} \equiv \langle n_{l\mu\uparrow} \rangle + \langle n_{l\mu\downarrow} \rangle$ and $\bar{m}_{\mu l} \equiv \langle n_{l\mu\uparrow} \rangle - \langle n_{l\mu\downarrow} \rangle$, plus a constant term that can be safely ig-
 75 nored. The average occupancies $\bar{n}_{\mu l}$ and magnetic moments $\bar{m}_{\mu l}$ are determined self-consistently.

76 We obtain the magnon spectrum of altermagnets by studying the transverse spin suscepti-
 77 bilities,

$$\chi_{\mu\nu}^{+-}(\vec{r}_{l'} - \vec{r}_l, t) \equiv -i\theta(t) \left\langle \left[S_{l\mu}^{+}(t), S_{l'\nu}^{-}(0) \right] \right\rangle \quad (3)$$

78 and

$$\chi_{\mu\nu}^{-+}(\vec{r}_{l'} - \vec{r}_l, t) \equiv -i\theta(t) \left\langle \left[S_{l\mu}^{-}(t), S_{l'\nu}^{+}(0) \right] \right\rangle, \quad (4)$$

79 where t is the time, $S_{l\mu}^{-} \equiv c_{l\mu\downarrow}^{\dagger} c_{l\mu\uparrow}$, ($S_{l\mu}^{+} = (S_{l\mu}^{-})^{\dagger}$) is the operator that creates a spin excitation
 80 with $S^z = -1$ ($S^z = 1$) at cell l in the sublattice μ , \vec{r}_l is the position of unit cell l , and $\theta(t)$
 81 is the Heaviside unit step function. These two-time correlation functions cannot be computed
 82 exactly for an interacting model such as the one defined in Eq. 1; the simplest approach that
 83 can describe magnons is the so-called random phase approximation (RPA), in which the inter-
 84 action is taken into account, to all orders in perturbation theory, between the electron and the
 85 hole that form the spin-flip excitation [10]. The RPA relates the transverse interacting suscep-
 86 tibilities χ^{\perp} ($\perp \equiv +- \text{ or } -+$) to the mean-field susceptibilities $\bar{\chi}^{\perp}$, which are the same Green
 87 functions defined in Eqs. 3 and 4, with the thermal average $\langle \cdot \rangle$ evaluated for the mean-field
 88 configuration. For the model considered here, after Fourier transforming both in time and
 89 position, the RPA equations are

$$\chi_{\mu\nu}^{+-}(\mathcal{Q}) = \bar{\chi}_{\mu\nu}^{+-}(\mathcal{Q}) - U \sum_{\xi} \bar{\chi}_{\mu\xi}^{+-}(\mathcal{Q}) \chi_{\xi\nu}^{+-}(\mathcal{Q}), \quad (5)$$

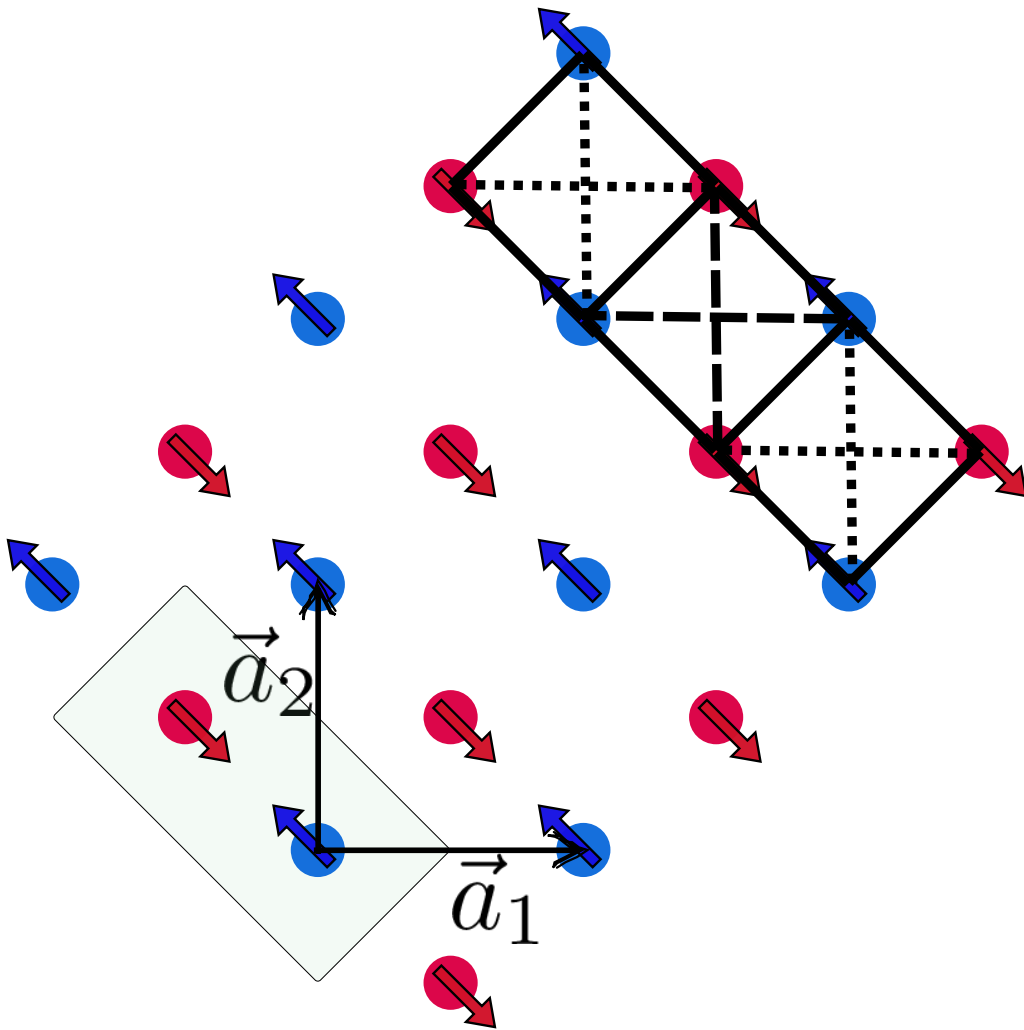


Figure 1: Schematic representation of the model altermagnet on a square lattice defined by primitive vectors \vec{a}_1 and \vec{a}_2 , with $|\vec{a}_1| = |\vec{a}_2| = a$. The solid line connecting blue and red sites represents the nearest neighbor hopping τ . Dashed and dotted lines represent the alternating second neighbor hoppings $\tau'(1 \pm \delta)$. The lightly colored rectangle indicates the unit cells.

90 where $\mathcal{Q} \equiv (\vec{q}, \hbar\Omega)$. We obtain an analogous expression for χ^{-+} . The spectral density associ-
 91 ated with magnons, projected on sublattice μ , is given by

$$\rho_{\mu}^{\perp}(\mathcal{Q}) = -\frac{1}{\pi} \text{Im} \chi_{\mu\mu}^{\perp}(\mathcal{Q}) \quad (6)$$

92 where \perp can be either $+-$ or $-+$, denoting the transversal character of these response functions
 93 with respect to the equilibrium staggered magnetization (Néel vector). Magnon energies $\hbar\Omega(\vec{q})$
 94 are associated with the positions of the peaks of ρ^{+-} (for the $S^z = -1$ magnons) or ρ^{-+} (for
 95 the $S^z = 1$ magnons), at fixed wave-vector \vec{q} . Analogously, magnon lifetimes are defined as
 96 the inverse of the full width at half-maximum of the magnon peaks.

97 2.1 Mean-field results

98 An insulating altermagnetic state can be obtained by choosing $U \gtrsim 3\tau$; however, for $3\tau \lesssim U \lesssim 10\tau$
 99 the mean-field configuration belongs to an intermediate coupling regime, for which the spin
 100 dynamics can not yet be properly described by a spin-only (Heisenberg-like) model. Thus, to
 101 benchmark our fermionic model against a spin model, we chose $U = 10\tau$, together with the
 102 hopping values $\tau' = 0.17\tau$ and $\delta = 0.83$. The self-consistent mean-field solution gives the
 103 bands shown in Fig. 6 of appendix A, with a staggered magnetic moment $m_A - m_B = 1.86\mu_B$
 104 per unit cell. For the reciprocal space path we plotted in Fig. 6, the spin splitting is zero only
 105 along the line $q_y = q_x$. Along the line $q_y = \frac{\pi}{a} - q_x$ there is the characteristic crossing between
 106 the \uparrow and \downarrow spin bands, associated with the altermagnetic symmetry.

107 The metallic altermagnetic state can be obtained either by tweaking the hopping param-
 108 eters, as shown in ref. [18], or by reducing the Hubbard parameter U . We chose the latter
 109 option to minimize the differences between the shapes of the electronic bands in the metallic
 110 and insulating states. By setting $\tau' = 0.17\tau$, $\delta = 0.83$ and $U = 2.5\tau$ we obtain the metal-
 111 lic altermagnetic bands shown in Fig. 6 of appendix A, with a staggered magnetic moment
 112 $m_A - m_B = 0.74\mu_B$ per unit cell.

113 3 Magnons

114 To benchmark our methodology, we first analyze the spin excitations of the insulating alter-
 115 magnet in the strong coupling limit ($U = 10\tau$), for which the spin model results should be
 116 valid [15, 19]. By scanning the spectral densities ρ^{+-} and ρ^{-+} in the $(\hbar\Omega, \vec{q})$ space we obtain
 117 the dispersion relations for $S^z = -1$ magnons ($+-$) and for $S^z = 1$ magnons ($-+$), shown in
 118 Fig. 2. The energy splitting between the two polarizations, one of the hallmarks of altermag-
 119 netism, is clearly seen along high-symmetry directions in the Brillouin zone. We also show
 120 the dispersion relation for (linearized) Holstein-Primakoff magnons, extracted from a Heisen-
 121 berg model for the altermagnet, including up to third-neighbor exchange. As expected, the
 122 agreement with the RPA treatment of the fermionic model is very good in this case ¹.

123 Along specific lines within the Brillouin zone we observe a behavior analogous to the “band
 124 inversion” associated with topologically non-trivial electronic bands. For instance, along the
 125 reciprocal space path going from $(\frac{\pi}{a}, 0)$ to $(0, \frac{\pi}{a})$ there is a crossing between the $S^z = -1$ and
 126 the $S^z = 1$ magnon branches. In the presence of spin-orbit coupling a gap may appear at
 127 the crossing point $(\frac{\pi}{2a}, \frac{\pi}{2a})$, possibly accompanied by a finite Berry curvature. This crossing is
 128 also associated with the peculiar directional behavior of altermagnetic magnons. If we focus
 129 on magnons with one S^z value we see that the energy at the $(\frac{\pi}{a}, 0)$ point in reciprocal space
 130 (thus, propagating along the x direction in real space with wavelength $\lambda = 2a$) is 40% different

¹This is contrast with the insulating intermediate coupling case, for which the spin model fails. See appendix D.

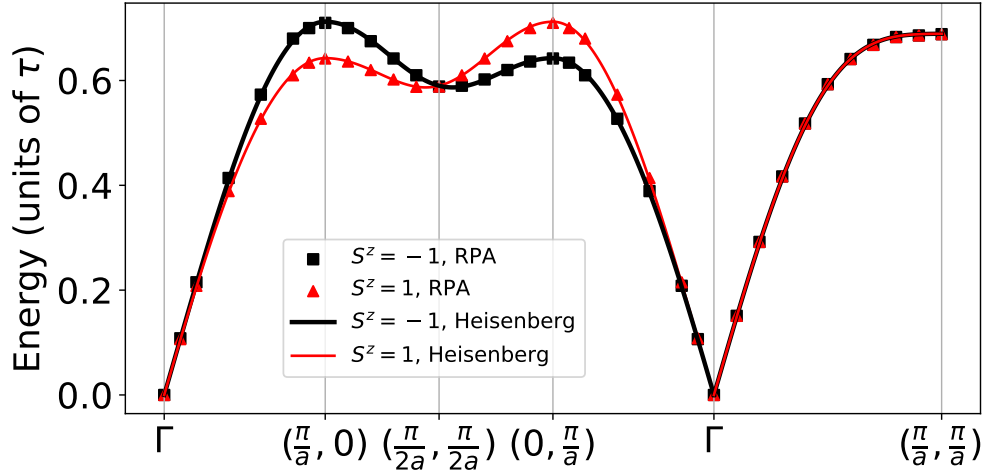


Figure 2: Dispersion relation for magnons in an insulating altermagnet in the strong coupling regime ($U = 10\tau$). The Heisenberg model used to fit the RPA energies includes up to third-neighbor exchange.

131 from that of a magnon with the same wavelength propagating along the y direction. This is
 132 illustrated in fig. 11 of the appendix E, where we plot the magnons spectral densities as a
 133 function of propagation direction, for a fixed wavelength. Combined with the fact that, for
 134 sufficiently small wavelengths (typically smaller than $\sim 5a$) magnons with a well-defined S^z
 135 are strongly sublattice-polarized, this feature may be exploited to guide magnons in spintronics
 136 devices.

137 3.1 Itinerant altermagnet

138 We now turn our attention to the behaviour of magnons in itinerant altermagnets. In con-
 139 trast to the insulating case, it can be expected that their lifetime is limited by Stoner damp-
 140 ing [10, 11, 20]. Magnons with energies exceeding single-particle spin-flip excitations (also
 141 known as Stoner excitations), can decay into the Stoner continuum [10]. The magnon life-
 142 time is inversely proportional to the density of Stoner modes, which is given by the imaginary
 143 part of the mean-field transverse susceptibility $\tilde{\chi}^\perp$. The effect of damping for a conducting
 144 altermagnet ($U = 2.5\tau$) is seen in the evolution of the spectral weight of spin excitations,
 145 shown along two different directions, (q, q) and $(q, 0)$ with $|q| < \frac{\pi}{a}$, in Figure 3a,b. For low
 146 energy, the spectral density has well defined peaks, whose position gives the magnon energy
 147 and the inverse of its linewidth gives the magnon lifetime. As the energies are increased, the
 148 peaks get broader and, above some energy threshold, they vanish into a continuum. Along the
 149 (q, q) direction, both $S_z = \pm 1$ excitations have the same spectral weight (fig. 3a). In contrast,
 150 along the $(q, 0)$ direction (fig. 3b), the $S^z = -1$ spin excitations have lorentzian spectral den-
 151 sities with relatively small linewidth in the whole wave number range, whereas the spectral
 152 density associated with the $S^z = 1$ spin excitations has a behavior similar to the (q, q) case.
 153 We thus find that, for itinerant altermagnets, magnons with a given S^z are only well defined
 154 along certain directions.

155 To make the connection between magnon lifetimes and density of Stoner modes, it is useful
 156 to plot both magnons' and Stoner excitations' spectral densities as color-coded functions of
 157 energy and wave number, shown in fig. 4. By following the bright spots in the top left panel, it
 158 is possible to trace dispersion relations for the $S^z = -1$ magnons, in analogy to the insulating
 159 case. For the $S^z = 1$ magnon, the bright spots disappear around $q \sim \frac{2\pi}{5a}$. This can be correlated

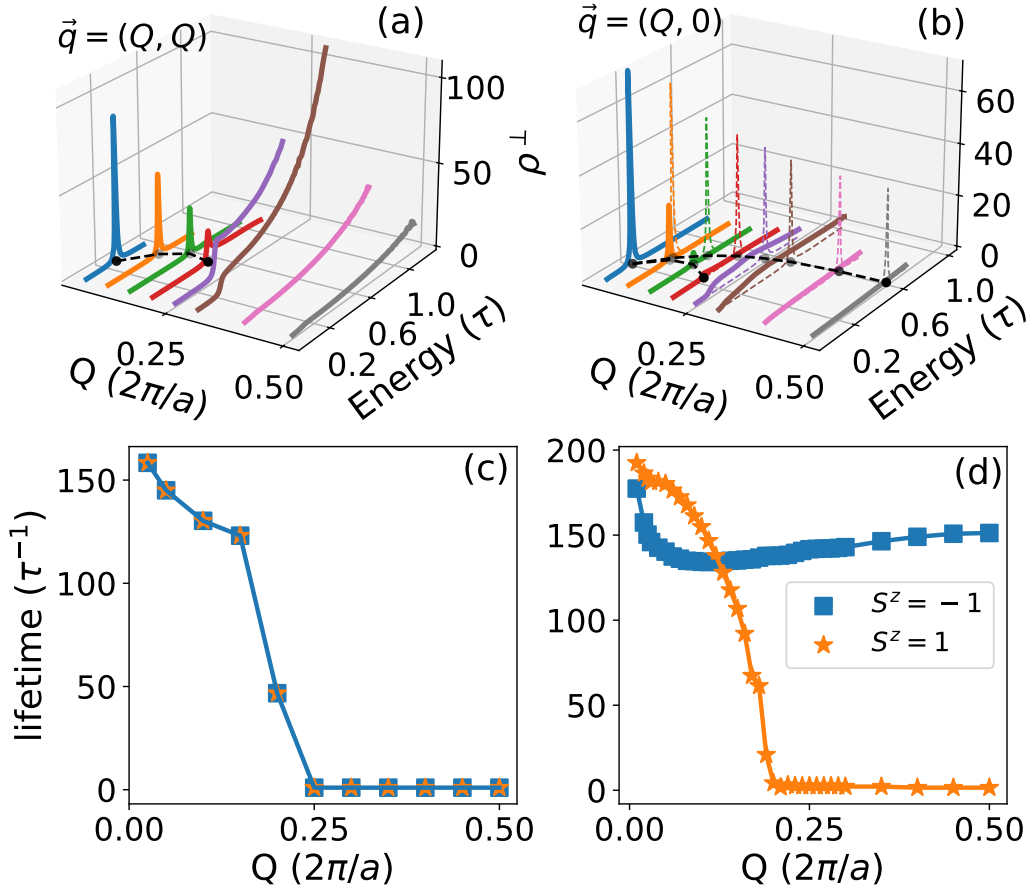


Figure 3: Top: spin excitation spectral densities in the metallic phase ($U = 2.5\tau$), along $\vec{q} = \frac{1}{\sqrt{2}}(q, q)$ (a) and $\vec{q} = (q, 0)$ (b), as a function of energy, for selected wave numbers. To improve visualization, the spectral density has been multiplied by 100 for the three largest wavenumbers ($q = 0.3, 0.4$ and 0.5), by 50 for $q = 0.25$ and by 5 for $q = 0.2$. In (b), solid lines correspond to ρ^{-+} , associated with the $S^z = 1$ spin excitations, and dashed lines correspond to ρ^{+-} , associated with the $S^z = -1$ spin excitations. Bottom: Lifetimes of the metallic magnons ($U = 2.5\tau$) propagating along the $\vec{q} = \frac{1}{\sqrt{2}}(q, q)$ (c) and $\vec{q} = (q, 0)$ (d), as a function of wave number, for $S^z = -1$ (squares) and $S^z = 1$ (stars) spin excitations.

160 with the boundaries of the Stoner continuum for $S^z = 1$ spin excitations, plotted in the bottom
 161 right panel. In contrast, the density of $S^z = -1$ Stoner modes is uniformly small over the
 162 whole wave number and energy ranges where $S^z = -1$ magnons exist. A detailed discussion
 163 of the origin of the density of Stoner modes in terms of the geometry of the spin-polarized
 164 Fermi surface pockets of the metallic altermagnet is presented in appendix C.

165 The giant magnon-lifetime anisotropy is better seen in a color-coded polar plot of the
 166 magnon spectral density, for a fixed wavelength. The angular variable indicates the propa-
 167 gation direction, and the radial variable is the magnon energy. In fig. 5 we show such a plot
 168 for $\lambda = \frac{10a}{3}$ (wave number $q = \frac{3\pi}{5a}$). The top-left panel shows the spectral density ρ_A^{+-} for
 169 $S^z = -1$ magnons, projected on sublattice A, and the top-right panel displays the equivalent
 170 quantity for sublattice B (ρ_B^{+-}). It is clear that $S^z = -1$ magnons are strongly suppressed
 171 for angles $\gtrsim 30^\circ$, and the $S^z = 1$ magnons for angles $\lesssim 60^\circ$. Such strong directionality is
 172 rarely seen for quasiparticles and elementary excitations, and is potentially very useful for ap-
 173 plications, especially when one considers the fact that magnons of wavelengths $\lambda \lesssim 4a$ live

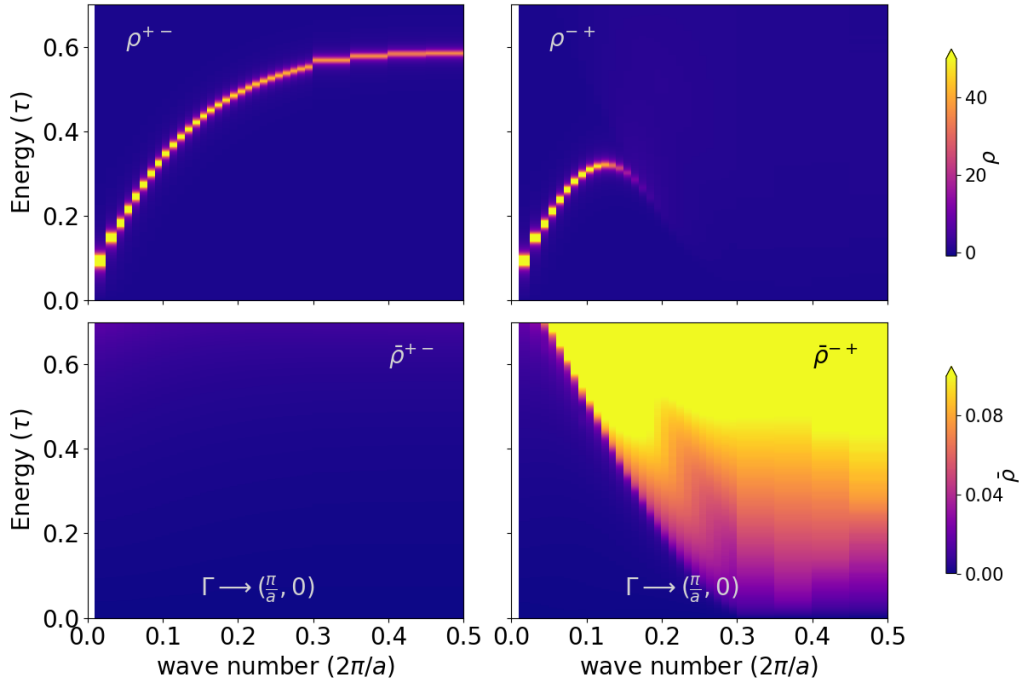


Figure 4: Top: Spectral densities for $S^z = -1$ (ρ^{+-} , left) and $S^z = 1$ (ρ^{-+} , right) metallic magnons ($U = 2.5\tau$) propagating along the x direction, as a function of wave number and energy. Bottom: Spectral densities for $S^z = -1$ ($\bar{\rho}^{+-}$, left) and $S^z = 1$ ($\bar{\rho}^{-+}$, right) Stoner excitations (single-particle spin flips) propagating along the x direction, as a function of wave number and energy.

174 preferentially in one of the sublattices. Thus, it is in principle possible to excite magnons along
 175 specific directions by choosing their excitation frequency and the sublattice to excite. Selec-
 176 tively addressing the sublattice may be challenging in systems where spin sublattices have
 177 atomic size, but not so much in synthetic magnets, where spin sublattices are associated with
 178 molecules containing tens of atoms [19, 21].

179 We have also considered the case of a doped insulating altermagnet, by choosing $U = 3.5\tau$
 180 and imposing an electronic occupation of 1.05 electrons per atomic site. In this case the
 181 anisotropic suppression of magnons is observed for propagation angles $30^\circ \lesssim \theta \lesssim 75^\circ$, as
 182 shown in the bottom panels of fig. 5. Thus, whenever it is possible to dope an insulating al-
 183 termagnet electrostatically, it is in principle also possible to control electrostatically the prop-
 184 agation direction of magnons.

185 The effects of a giant spatial anisotropy in magnon lifetimes are likely to be noticed on
 186 several transport coefficients of metallic altermagnets [22]. Electronic transport is expected to
 187 be impacted by electron-magnon scattering, especially at low temperatures. Moreover, with
 188 current high-resolution spin-polarized electron energy loss spectroscopy [23, 24] it should be
 189 possible to probe experimentally the lifetime anisotropy predicted by our theoretical analysis.

190 We would like to emphasize that the lifetimes of magnons in itinerant magnets is related
 191 to the frequency and wave-vector dependent spectral density of Stoner modes, as detailed in
 192 the appendix B. The authors of a previous work [9] have estimated the relative intensity of
 193 magnon damping, as a function of magnon wave vector only, by integrating the spectral density
 194 of Stoner excitations over the whole magnon band width. This quantity can not be associated
 195 with the lifetime of individual magnons, although it can give an idea of the overall importance
 196 of Stoner excitations for the magnon spectrum. The relevant quantity for determining the
 197 lifetime of a magnon with well-defined energy and momentum is the mean-field transverse

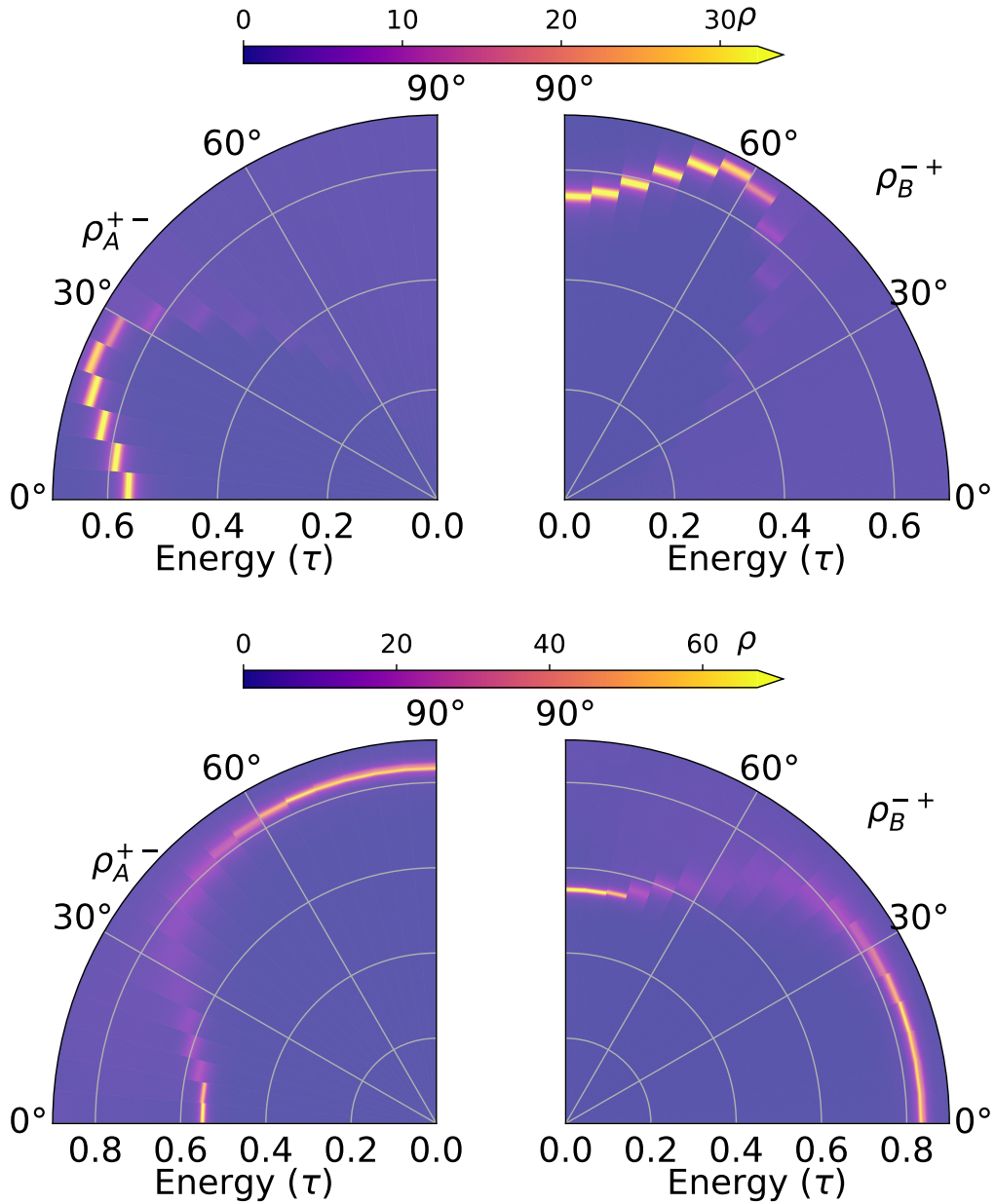


Figure 5: Magnon spectral densities as functions of propagation angle, for a fixed wavelength ($\frac{10a}{3}$). The radial variable represents energy (in units of the nearest-neighbor hopping τ). ρ_A^{+-} corresponds to $S^z = -1$ magnons, ρ_B^{-+} corresponds to $S^z = 1$ magnons. Top panels: metallic phase ($U = 2.5\tau$); bottom panels: doped insulating phase ($U = 3.5\tau$, excess 0.1 electrons per unit cell).

198 spin susceptibility calculated at the energy of the magnon (the pole of the RPA transverse spin
199 susceptibility), as discussed in appendix B.

200 4 Conclusion

201 We have studied the intrinsic damping of magnons in altermagnets. These collective modes
202 come with two values of $S_z = \pm 1$. Contrary to their counterparts in ferro- and antiferromag-
203 nets, we find a giant spatial anisotropy of magnon lifetimes in itinerant altermagnets. We find
204 that, for a given direction, only magnons with a given sign of S_z survive without melting due
205 to Stoner damping. The ultimate reason for this unique behaviour relies on the existence of
206 spin-polarized Fermi surface pockets that characterizes altermagnets. Therefore, we expect
207 our predictions are generic of all itinerant altermagnets, rather than model specific and will
208 have to be considered in future magnonic applications.

209 Acknowledgments

210 A.T.C. acknowledges fruitful discussions with D. L. R. Santos. The authors acknowledge finan-
211 cial support from FCT (Grant No. PTDC/FIS-MAC/2045/2021), SNF Sinergia (Grant Pimag,
212 CRSII5_205987) the European Union (Grant FUNLAYERS - 101079184). J.F.-R. acknowledges
213 financial funding from Generalitat Valenciana (Prometeo2021/017 and MFA/2022/045), Span-
214 ish Government through PID2022-141712NB-C22, and the Advanced Materials programme
215 supported by MCIN with funding from European Union NextGenerationEU (PRTR-C17.I1)
216 and by Generalitat Valenciana (MFA/2022/045).

217 A Mean-field electronic structure

218 We present the electronic bands corresponding to the mean-field configurations considered in
219 the letter: strong-coupling insulating ($U = 10\tau$, fig. 6, left panel), metallic ($U = 2.5\tau$, fig 6,
220 right panel), and slightly doped insulating ($U = 3.5\tau$, fig. 7, right panel). Both metallic and
221 insulating phases have half-filled bands (one electron per lattice site), whereas the doped phase
222 has 1.05 electrons per lattice site. Table 1 shows the values of the Hamiltonian parameters
223 associated with the different phases, as well as the mean-field staggered magnetic moment
224 per unit cell. We also show the intermediate-coupling insulating case ($U = 3.5\tau$, fig. 7, left
225 panel).

	τ'	δ	U	$ m_\uparrow - m_\downarrow (\mu_B)$
Insulating (strong coupling)	0.16	0.83	10	1.86
Insulating (intermediate coupling)	0.16	0.83	3.5	1.28
Metallic	0.16	0.83	2.5	0.74

Table 1: Values for the Hamiltonian parameters (in units of the nearest-neighbor hopping τ) used in this work, and respective staggered magnetic moment per unit cell, in units of Bohr magnetons μ_B .

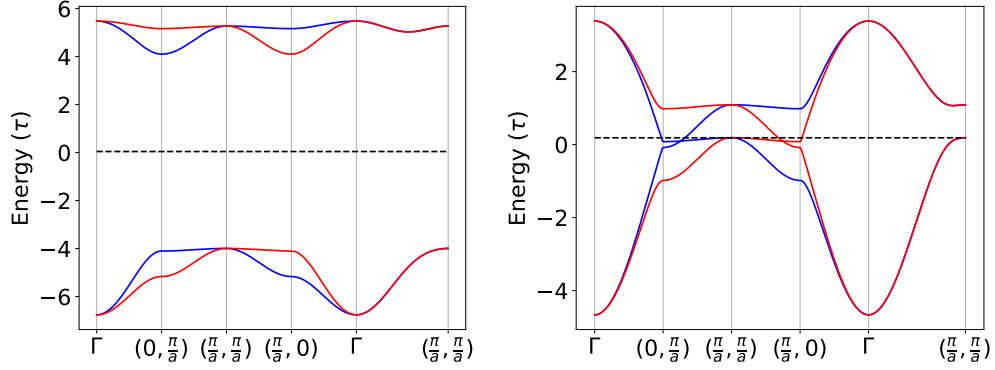


Figure 6: Electron energy bands for the strong-coupling insulating (left panel, $U = 10\tau$) and metallic (right panel, $U = 2.5\tau$) mean-field ground state configuration of the altermagnet Hamiltonian (eq. 1 of the main text), with $\tau' = 0.16\tau$ and $\delta = 0.83$. Red and blue lines represent \uparrow and \downarrow spin sub-bands. The black dashed line marks the Fermi energy.

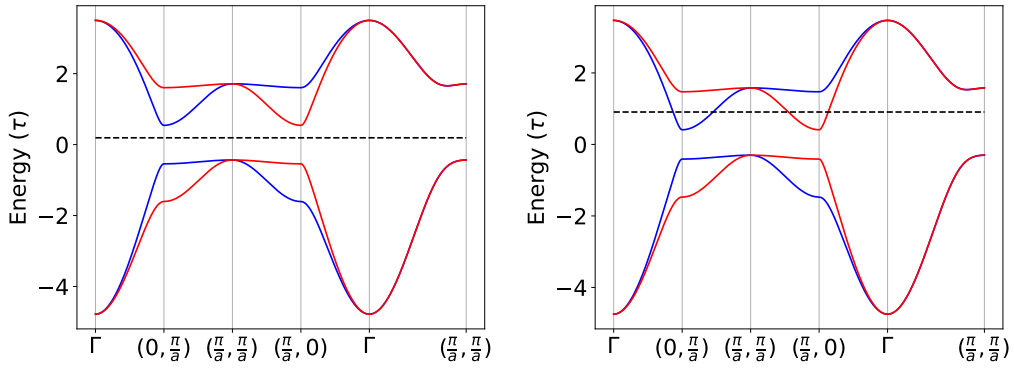


Figure 7: Electron energy bands for the mean-field ground state configuration of the altermagnet Hamiltonian (eq. 1 of the main text) in the insulating intermediate coupling regime ($U = 3.5\tau$) at half-filling (left panel) and away from half-filling (1.05 electrons per lattice site, right panel). The values for the hopping parameters are $\tau' = 0.16\tau$, $\delta = 0.83$. Red and blue lines represent \uparrow and \downarrow spin sub-bands. The black dashed line marks the Fermi energy.

226 B Relationship between the density of Stoner modes and the magnon 227 lifetime

228 The standard random phase approximation (RPA) applied to the transverse spin susceptibility
229 of a Hubbard Hamiltonian results in a relationship between the magnon Green function χ^{+-}
230 and the mean-field Green function $\bar{\chi}^{+-}$,

$$\chi^{+-}(\vec{q}, \hbar\Omega) = \frac{\bar{\chi}^{+-}(\vec{q}, \hbar\Omega)}{1 + U\bar{\chi}^{+-}(\vec{q}, \hbar\Omega)}. \quad (\text{B.1})$$

231 We would like to cast this expression in a form that resembles a Green function with a self-
232 energy correction,

$$G = \frac{1}{\bar{G}^{-1} + \Sigma}, \quad (\text{B.2})$$

233 where \bar{G} is the bare Green function and Σ is the self-energy. For this it is useful to split all
234 quantities into their real and imaginary parts, denoted below by R and I subscripts. The real
235 and imaginary parts of the magnon Green function then become (we will omit the energy and
236 wave vector arguments for now to avoid cluttering the expressions)

$$\begin{aligned} \text{Re}[\chi^{+-}] &= \frac{\bar{\chi}_R^{+-}(1 + U\bar{\chi}_R^{+-}) + U(\bar{\chi}_I^{+-})^2}{(1 + U\bar{\chi}_R^{+-})^2 + (U\bar{\chi}_I^{+-})^2}, \\ \text{Im}[\chi^{+-}] &= \frac{\bar{\chi}_I^{+-}}{(1 + U\bar{\chi}_R^{+-})^2 + (U\bar{\chi}_I^{+-})^2}. \end{aligned} \quad (\text{B.3})$$

237 Similarly,

$$\begin{aligned} \text{Re}[G] &= \frac{\bar{G}^{-1} + \Sigma_R}{(\bar{G}^{-1} + \Sigma_R)^2 + \Sigma_I^2}, \\ \text{Im}[G] &= -\frac{\Sigma_I}{(\bar{G}^{-1} + \Sigma_R)^2 + \Sigma_I^2}. \end{aligned} \quad (\text{B.4})$$

238 By comparing the imaginary parts of the generic Green function G to $\text{Im}[\chi^{+-}]$ we notice
239 immediately a clear analogy between $U\bar{\chi}_I^{+-}$ and Σ_I . Notice also that, as in the electronic case,
240 magnon damping is inextricably tied to shifts in magnon energy, through the real part of the
241 self-energy Σ_R . It is clear, then, that the lifetime of a magnon with wave vector \vec{q} and energy
242 $\hbar\Omega(\vec{q})$ is determined by the spectral density of Stoner modes with wave vector \vec{q} and energy
243 $\hbar\Omega(\vec{q})$.

244 C Origin of the anisotropic magnon lifetime

245 To further shed light on the mechanism behind the lifetime anisotropy of metallic magnons,
246 it is useful to look at constant energy contours of the electronic bands in the mean-field al-
247 termagnetic configuration. The goal is to identify qualitatively the direction dependence of
248 single-particle spin-flip transitions that give rise to the anisotropic density of Stoner modes.
249 In figure 8 we show three constant energy contours for each spin direction, blue contours for
250 \uparrow spin electrons, red contours for \downarrow . In the left panel we show contours for occupied \uparrow states
251 (including the Fermi contour at zero energy) and unoccupied \downarrow states (also including the Fermi
252 contour at zero energy), relevant for $S^z = -1$ spin flips ($\downarrow \rightarrow \uparrow$). Thus, in the left panel we
253 can identify possible single-particle spin-flip transitions by connecting blue and red contours.

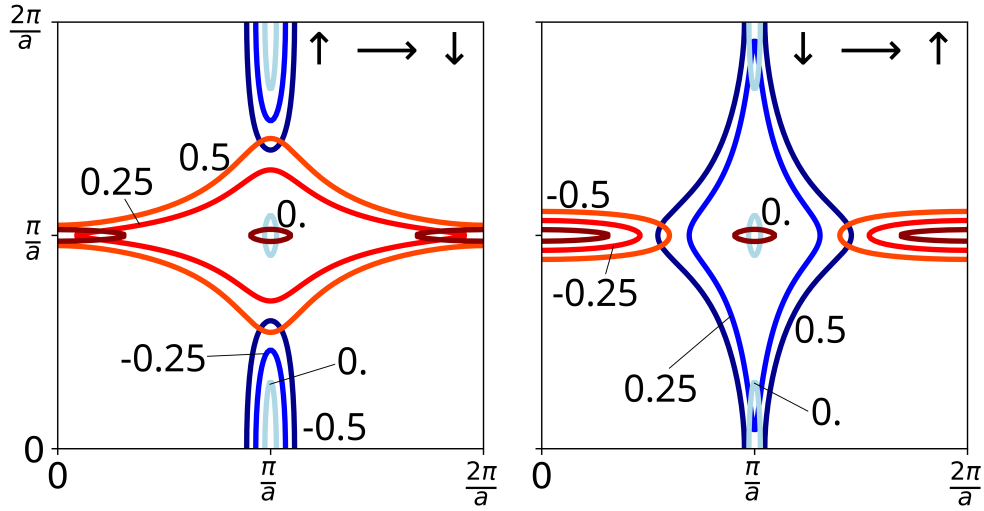


Figure 8: Contours of the electronic bands around the Fermi level; blue curves are for \uparrow spin bands, red curves for \downarrow . Left panel ($\uparrow \rightarrow \downarrow$): occupied \uparrow states (shades of blue, at energies $E_F - 0.5\tau$, $E_F - 0.25\tau$ and E_F) and unoccupied \downarrow states (shades of red, E_F , $E_F + 0.25\tau$ and $E_F + 0.5\tau$). Right panel ($\downarrow \rightarrow \uparrow$): occupied \downarrow states (shades of red, at energies $E_F - 0.5\tau$, $E_F - 0.25\tau$ and E_F) and unoccupied \uparrow states (shades of blue, E_F , $E_F + 0.25\tau$ and $E_F + 0.5\tau$).

254 In the left panel we see that, apart from the very small pockets at $(\frac{\pi}{a}, \frac{\pi}{a})$, there is no horizontal
 255 line connecting blue and red contours. The consequence is that the density of $S^z = -1$
 256 Stoner modes with wave vectors along the x direction is very small, and $S^z = -1$ magnons
 257 propagating along the x direction are long-lived. On the other hand, there are plenty of con-
 258 nections between blue and red contours at angles $\gtrsim 30^\circ$, meaning that magnons propagating
 259 along those directions will be substantially damped. In the right panel we show the analogous
 260 information for $S^z = 1$ spin flips ($\downarrow \rightarrow \uparrow$): occupied \downarrow states (including the Fermi contour at
 261 zero energy) and unoccupied \uparrow states (also including the Fermi contour at zero energy). Now
 262 it is clear that there are many possible single- particle spin-flip transitions with wave vectors
 263 along x , whereas very few with wave vectors along y , thus meaning that $S^z = 1$ magnons are
 264 strongly damped when propagating along x but long-lived when propagating along x .

265 D Insulating altermagnet in the intermediate coupling regime ($U = 3.5\tau$).

266 As mentioned in the main main text, the insulating altermagnetic phase of the model is ob-
 267 tained for $U \gtrsim 3\tau$. In this regime, although the electronic bands are clearly those of an
 268 altermagnetic insulator (see the left panel of figure 7), the magnons bear marks of itinerant
 269 magnetism, especially at short wavelengths. A clear signature of itinerant behavior is the fact
 270 that the magnon lineshape acquires a finite linewidth and, at large enough energies, deviates
 271 significantly from a lorentzian shape. This is seen in fig. 10 for a short wavelength magnon
 272 ($\lambda = 2a$) propagating along the x direction. The lineshape of the $S^z = 1$ magnon (right panel)
 273 is very close to a lorentzian (dashed orange line). In contrast, the lineshape of the higher
 274 energy $S^z = -1$ magnon (left panel) is clearly not a lorentzian.

275 Another consequence of the coupling between magnons and Stoner excitations is a renor-
 276 malization of magnon energies relative to those predicted by a localized spin model. In fig. 9
 277 we compare the dispersion relation of magnons for the insulating altermagnet in the inter-
 278 mediate coupling regime, extracted from the fermionica model, to the energies of linearized

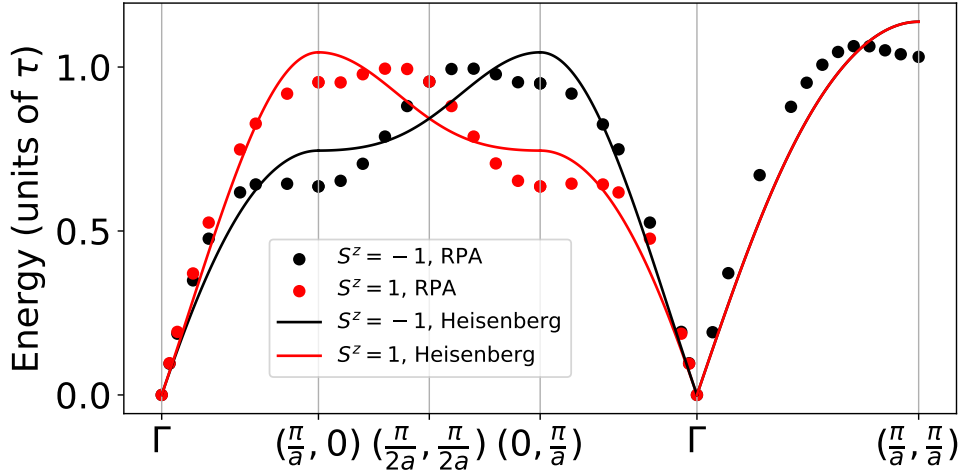


Figure 9: Dispersion relation for magnons in an insulating altermagnet in the intermediate coupling regime ($U = 3.5\tau$). The Heisenberg model used to fit the RPA energies includes up to third-neighbor exchange.

279 Holstein-Primakoff magnons of a localized spins model, with exchanges up to third neighbors.
 280 The exchange parameters of the localized spin model have been obtained from a fit to the
 281 fermionic model energies. Although the main qualitative features of the dispersion are cap-
 282 tured by the localized spins model, it does a poor job of matching quantitatively the magnon
 283 energies over the whole Brillouin zone, since the spin only model cannot capture the renor-
 284 malization of the magnon energies by Stoner excitations.

285 To illustrate the effect of the coupling to the Stoner continuum we plot, in fig. 10, the
 286 spectral densities for magnons with $S^z = -1$ (ρ^{+-}) and $S^z = 1$ (ρ^{-+}). Notice that the lineshape
 287 of the $S^z = -1$ magnon (left panel) is clearly not a lorentzian, whereas the $S^z = 1$ magnon is
 288 well fitted by a lorentzian with a finite linewidth, denoting a finite lifetime.

289 E Directionality of the magnon spectrum in the insulating regime 290 (intermediate coupling).

291 Here we illustrate the directional dependence of the magnon energies for the intermediate
 292 coupling ($U = 3.5\tau$) insulating case (figure 11). The main difference between this case and
 293 the metallic and slightly doped cases is that the magnons appear as well-defined collective
 294 excitation for all directions of propagations (compare with fig. 5 of the main text).

295 A very good agreement between the predictions of the fermionic model and those of the
 296 spin-only model is expected for insulating magnets in general; here the less-than-perfect agree-
 297 ment can be partially attributed to the influence of Stoner excitations for wave vectors close
 298 to the edges of the Brillouin zone. Fig. XXX in the SM shows that the spectral density for high-
 299 energy, short wavelength magnons are significantly broadened, a consequence of damping by
 300 Stoner excitations. [11, 20] Another possible reason for the disagree-

301 This is due to the continuum of Stoner modes with vanishingly small energies and wave
 302 numbers, coming from states around the two Fermi surface pockets with opposite spins cen-
 303 tered at $(\frac{\pi}{a}, \frac{\pi}{a})$ (see Fig. 8 of appendix C). As the magnon energy increases (and wavelength
 304 decreases), the lifetime of one of the polarizations has a slight monotonic decrease over the
 305 whole energy range, while for the opposite polarization it has similar behaviour up to $\lambda \lesssim 4a$,

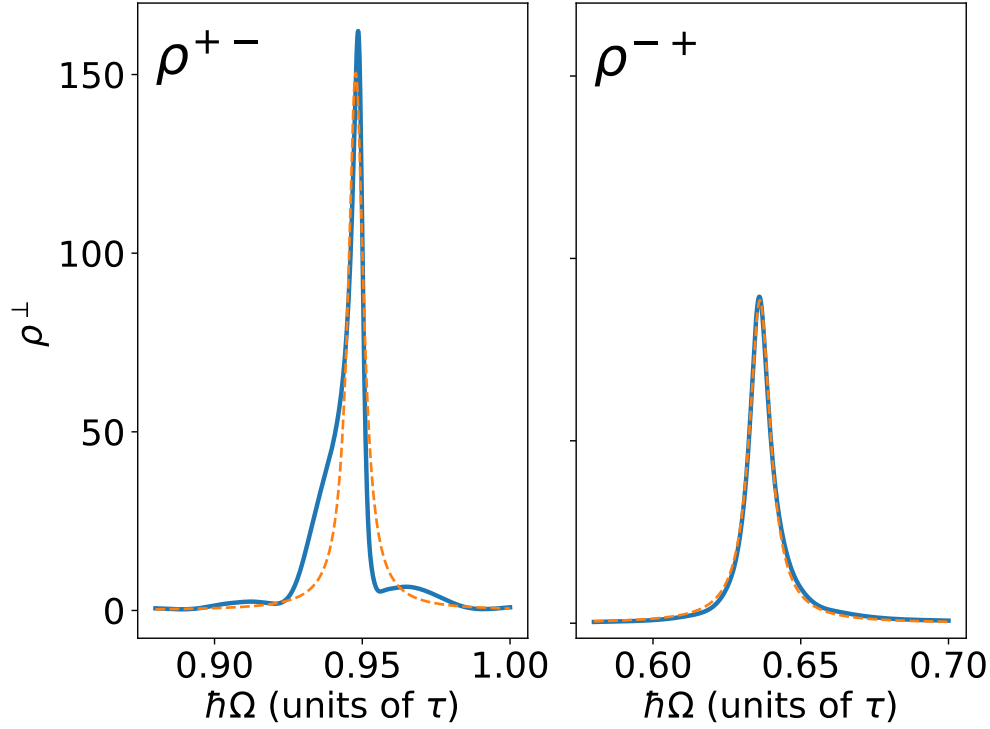


Figure 10: Spectral density of insulating magnons in the intermediate regime ($U = 3.5\tau$), for wave vector $\vec{q} = (\frac{\pi}{a}, 0)$. The left and right panels correspond to $S^z = -1$ and $S^z = 1$ magnons, respectively.

306 where the lineshape starts to change drastically, leading to the disappearance of the magnon
 307 signal altogether. This is shown in fig. 4 for propagation along the x direction. In fact, the
 308 shape of ρ^{-+} deviates so much from the Lorentzian shape (associated with long-lived quasi-
 309 particles) that the $S^z = 1$ magnon essentially vanishes. This time the culprit is the Stoner
 310 continuum associated with single-particle excitations from the \downarrow states around $(\frac{\pi}{a}, 0)$ to the
 311 \uparrow states around $(\frac{\pi}{a}, \frac{\pi}{a})$, whose spectral density is shown in the right bottom panel of fig. 4).
 312 The large spectral density for these single-particle spin flip excitations occur for wave vectors
 313 predominantly pointing along the x direction, thus producing highly anisotropic, polarization
 314 dependent damping rates. In contrast, the spectral density for single-particle excitations with
 315 $S^z = -1$ propagating along x , shown in the left-bottom panel of fig. 4, is very small over the
 316 whole $(q_x, \hbar\Omega)$ plane. This ensures the $S^z = -1$ magnons propagating along x are well-defined
 317 collective excitations over their whole bandwidth. For magnons propagating along y the picture
 318 is reversed, with $S^z = -1$ magnons strongly suppressed for wavelengths $\lambda \lesssim 5a$.

319 For wave vectors along the line $q_x = q_y$, where magnons of both polarizations are de-
 320 generate, the spectral densities for both $S^z = \pm 1$ magnons become featureless for $\lambda \lesssim 4a$,
 321 indicating that magnons along that direction are completely suppressed by damping. This is
 322 shown in fig. 3a, where we plot the spectral density as a function of energy for selected wave
 323 numbers. Once again, this suppression can be understood as a result of critical damping by
 324 the Stoner continua connecting states around the Fermi surface pockets centered at $(0, \frac{\pi}{a})$ and
 325 $(\frac{\pi}{a}, 0)$ to the states around the Fermi pocket centered at $(\frac{\pi}{a}, \frac{\pi}{a})$. In this case, though, both
 326 single-particle spin flips are allowed, $\uparrow \rightarrow \downarrow$ and $\downarrow \rightarrow \uparrow$.

References

- 327
- 328 [1] L.-D. Yuan, Z. Wang, J.-W. Luo, E. I. Rashba and A. Zunger, *Giant momentum-dependent*
329 *spin splitting in centrosymmetric low-z antiferromagnets*, Phys. Rev. B **102**, 014422
330 (2020), doi:[10.1103/PhysRevB.102.014422](https://doi.org/10.1103/PhysRevB.102.014422).
- 331 [2] L. Šmejkal, J. Sinova and T. Jungwirth, *Emerging research landscape of altermagnetism*,
332 Phys. Rev. X **12**, 040501 (2022), doi:[10.1103/PhysRevX.12.040501](https://doi.org/10.1103/PhysRevX.12.040501).
- 333 [3] L. Šmejkal, J. Sinova and T. Jungwirth, *Beyond conventional ferromagnetism and antifer-*
334 *romagnetism: A phase with nonrelativistic spin and crystal rotation symmetry*, Phys. Rev.
335 X **12**, 031042 (2022), doi:[10.1103/PhysRevX.12.031042](https://doi.org/10.1103/PhysRevX.12.031042).
- 336 [4] S. I. Pekar and E. I. Rashba, *Combined resonance in crystals in inhomogeneous magnetic*
337 *fields*, Zh. Eksp. Teor. Fiz. **47**, 1927 (1964).
- 338 [5] T. A. Maier and S. Okamoto, *Weak-coupling theory of neutron scattering as a probe of al-*
339 *termagnetism*, Phys. Rev. B **108**, L100402 (2023), doi:[10.1103/PhysRevB.108.L100402](https://doi.org/10.1103/PhysRevB.108.L100402).
- 340 [6] S. Sarkar, R. Capu, Y. G. Pashkevich, J. Knobel, M. R. Cantarino, A. Nag, K. Kummer,
341 D. Betto, R. Sant, C. W. Nicholson, J. Khmaladze, K.-J. Zhou *et al.*, *Composite anti-*
342 *ferromagnetic and orbital order with altermagnetic properties at a cuprate/manganite in-*
343 *terface*, PNAS Nexus **3**(4), pgae100 (2024), doi:[10.1093/pnasnexus/pgae100](https://doi.org/10.1093/pnasnexus/pgae100), <https://academic.oup.com/pnasnexus/article-pdf/3/4/pgae100/57469478/pgae100.pdf>.
- 344
- 345 [7] Y. Takahashi, *Spin fluctuation theory of itinerant electron magnetism*, Springer Tracts in
346 Modern Physics. Springer, Berlin (2013).
- 347 [8] S. M. Rezende, S. M. Rezende, A. Azevedo, A. Azevedo, A. Azevedo, R. L. Rodríguez-
348 Suárez and R. L. Rodríguez-Suárez, *Introduction to antiferromagnetic magnons*, J. Appl.
349 Phys. (2019), doi:[10.1063/1.5109132](https://doi.org/10.1063/1.5109132).
- 350 [9] L. Šmejkal, A. Marmodoro, K.-H. Ahn, R. González-Hernández, I. Turek, S. Mankovsky,
351 H. Ebert, S. W. D'Souza, O. Šipr, J. Sinova and T. Jungwirth, *Chiral magnons in altermag-*
352 *netic RuO_2* , Phys. Rev. Lett. **131**, 256703 (2023), doi:[10.1103/PhysRevLett.131.256703](https://doi.org/10.1103/PhysRevLett.131.256703).
- 353 [10] S. Doniach and E. Sondheimer, *Green's Functions for Solid State Physicists*, Imperial
354 College Press, ISBN 9781860940804 (1998).
- 355 [11] L. H. M. Barbosa, R. B. Muniz, A. T. Costa and J. Mathon, *Spin waves in ultrathin ferro-*
356 *magnetic overlayers*, Phys. Rev. B **63**, 174401 (2001), doi:[10.1103/PhysRevB.63.174401](https://doi.org/10.1103/PhysRevB.63.174401).
- 357 [12] E. Michel, H. Ibach, C. M. Schneider, D. L. R. Santos and A. T. Costa, *Lifetime and*
358 *mean free path of spin waves in ultrathin cobalt films*, Phys. Rev. B **94**, 014420 (2016),
359 doi:[10.1103/PhysRevB.94.014420](https://doi.org/10.1103/PhysRevB.94.014420).
- 360 [13] F. Garcia-Gaitan, A. Kefayati, J. Q. Xiao and B. K. Nikolic, *Magnon spectrum of altermag-*
361 *nets: Time-dependent matrix product states vs. linearized holstein-primakoff calculations*
362 *unravelling spontaneous magnon decay* (2024), [2402.19433](https://arxiv.org/abs/2402.19433).
- 363 [14] J. Sødequist and T. Olsen, *Two-dimensional altermagnets from high throughput compu-*
364 *tational screening: symmetry requirements, chiral magnons and spin-orbit effects* (2024),
365 [2401.05992](https://arxiv.org/abs/2401.05992).
- 366 [15] P. M. Cønsoli and M. Vojta, *$Su(3)$ altermagnetism: Lattice models, chiral magnons, and*
367 *flavor-split bands* (2024), [2402.18629](https://arxiv.org/abs/2402.18629).

- 368 [16] E. W. Hodt and J. Linder, *Spin pumping in an altermagnet/normal metal bilayer* (2023),
369 [2310.15220](https://arxiv.org/abs/2310.15220).
- 370 [17] A. E. Kanj, O. Gomonay, I. Boventer, P. Bortolotti, V. Cros, A. Anane and R. Lebrun, *Antiferromagnetic magnon spintronic based on nonreciprocal and nondegenerated ultra-fast spin-waves in the canted antiferromagnet Fe_2O_3* ,
371 *Science Advances* **9**(32), eadh1601 (2023), doi:[10.1126/sciadv.adh1601](https://doi.org/10.1126/sciadv.adh1601), <https://www.science.org/doi/pdf/10.1126/sciadv.adh1601>.
372
373
374
- 375 [18] P. Das, V. Leeb, J. Knolle and M. Knap, *Realizing altermagnetism in fermi-hubbard models with ultracold atoms* (2023), [2312.10151](https://arxiv.org/abs/2312.10151).
376
- 377 [19] G. Catarina, J. C. G. Henriques, A. Molina-Sánchez, A. T. Costa and J. Fernández-Rossier, *Broken-symmetry magnetic phases in two-dimensional triangulene crystals*, *Phys. Rev. Res.*
378 **5**, 043226 (2023), doi:[10.1103/PhysRevResearch.5.043226](https://doi.org/10.1103/PhysRevResearch.5.043226).
379
- 380 [20] A. T. Costa, R. B. Muniz and D. L. Mills, *Spin waves and their damping in itinerant ultrathin ferromagnets: Intermediate wave vectors*, *Phys. Rev. B* **74**, 214403 (2006),
381 doi:[10.1103/PhysRevB.74.214403](https://doi.org/10.1103/PhysRevB.74.214403).
382
- 383 [21] Y. Liu, J. Yu and C.-C. Liu, *Twisted magnetic van der waals bilayers: An ideal platform for altermagnetism* (2024), [2404.17146](https://arxiv.org/abs/2404.17146).
384
- 385 [22] I. Žutić, J. Fabian and S. Das Sarma, *Spintronics: Fundamentals and applications*, *Rev. Mod. Phys.* **76**, 323 (2004), doi:[10.1103/RevModPhys.76.323](https://doi.org/10.1103/RevModPhys.76.323).
386
- 387 [23] K. Zakeri and C. Berthod, *Theory of spin-polarized high-resolution electron energy loss spectroscopy from nonmagnetic surfaces with a large spin-orbit coupling*, *Phys. Rev. B* **106**,
388 235117 (2022), doi:[10.1103/PhysRevB.106.235117](https://doi.org/10.1103/PhysRevB.106.235117).
389
- 390 [24] K. Zakeri, D. Rau, J. Jandke, F. Yang, W. Wulfhchel and C. Berthod, *Direct probing of a large spin-orbit coupling in the fese superconducting monolayer on sto*, *ACS Nano* **17**(10),
391 9575 (2023), doi:[10.1021/acsnano.3c02876](https://doi.org/10.1021/acs.nano.3c02876), PMID: 37155694, <https://doi.org/10.1021/acsnano.3c02876>.
392
393

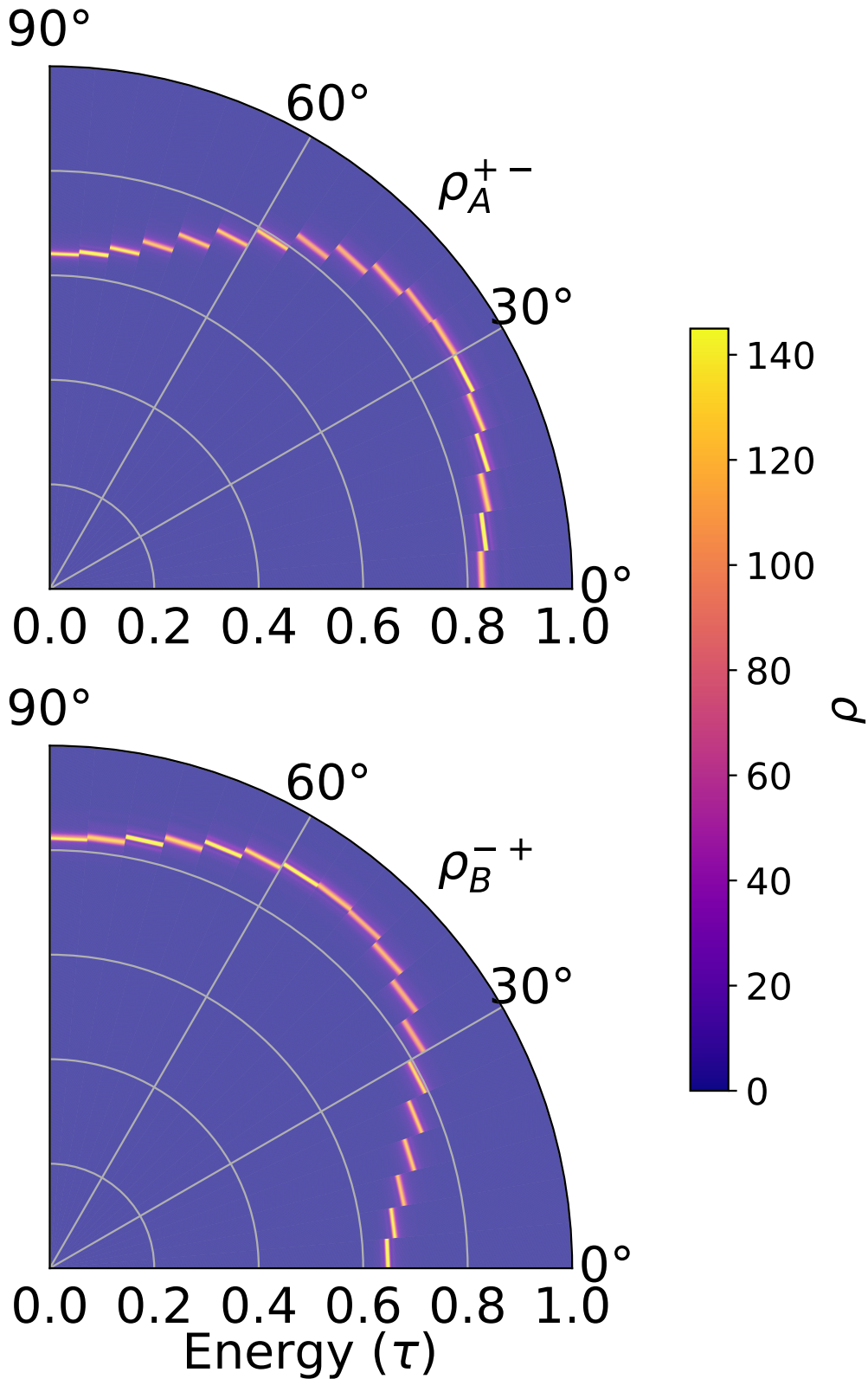


Figure 11: **Directionality of magnons in an insulator.** We plot the magnon spectral densities, as a function propagation angle, for a fixed wavelength ($\frac{10a}{3}$) for an insulating altermagnet. The top panel shows ρ_A^{+-} (for the $S^z = -1$ polarization) and the bottom panel shows ρ_B^{-+} (for the $S^z = -1$ polarization). The radial variable represents energy (in units of the nearest-neighbor hopping τ).